Journal of Physical Organic Chemistry

WILEY

Journal of Physical Organic Chemistry

RESEARCH ARTICLE

Antiradical Potency of Diphlorethol: DFT (Density Functional Theory), Molecular Docking, and ADMET Profile

Chu Anh Van[1] | Tran Quang Hai[2] | Nguyen Xuan Ha[3] | Nguyen Thi Hanh[1] | Nguyen Ngoc Linh[4] | Ninh The Son[5]

[1]Faculty of Chemistry, Hanoi Pedagogical University 2 (HPU2), Phucyen, Vinhphuc, Vietnam | [2]Faculty of Chemical Technology, Hanoi University of Industry, Hanoi, Vietnam | [3]Institute of Natural Products Chemistry, Vietnam Academy of Science and Technology (VAST), Hanoi, Vietnam | [4]Faculty of Pharmacy, Thanh Do University, Hanoi, Vietnam | [5]Institute of Chemistry, Vietnam Academy of Science and Technology (VAST), Hanoi, Vietnam

Correspondence: Ninh The Son (ntson@ich.vast.vn)

Received: 15 April 2025 | **Revised:** 25 June 2025 | **Accepted:** 26 June 2025

Funding: The authors received no specific funding for this work.

Keywords: ADMET | antioxidant | density functional theory | diphlorethol | docking

ABSTRACT

Diphlorethol is a typical phlorotannin with multipharmacological activities. However, its antiradical activity is still ambiguous. The current study aims to evaluate its radical scavenging using thermodynamics and kinetics-based density functional theory (DFT) calculations. The results indicated that the main radical scavenging mechanism in gas and lipid was the formal hydrogen transfer (FHT), and that for the aqueous medium was the sequential proton loss-electron transfer (SPLET). The kinetic reactions with $HOO^{\cdot}$ and $CH_3OO^{\cdot}$ radicals resulted in the $k_{overall}$ (overall rate constant) of 1.2×10^{8}–$1.6\times10^{8}\,M^{-1}s^{-1}$ in water and 3.0×10^{0}–$2.7\times10^{1}\,M^{-1}s^{-1}$ in pentyl ethanoate. 4- and 6-OH acted as active centers for radical scavenging. The molecular docking simulation suggested that diphlorethol could serve as a potential inhibitor of the oxidative activity of the Keap1 enzyme, particularly through its interaction with the crucial amino acid residue Arg415. The ADMET (absorption, distribution, metabolism, excretion, and toxicity) analysis demonstrated that diphlorethol exhibited favorable pharmacokinetic properties, including good water solubility, high intestinal absorption, and moderate tissue distribution. Diphlorethol did not induce hepatotoxicity or skin sensitization and showed no inhibitory effects on hERG I or hERG II channels, supporting its potential as a safe antioxidant candidate for further development.

1 | Introduction

Atoms or molecules with one or more unpaired electrons are referred to be free radicals. Many xenobiotics are toxic since they activate other compounds metabolically, producing free radicals or reactive oxygen species (ROS), such as peroxyl radicals ($ROO^{\cdot}$), hydroxyl radicals ($^{\cdot}OH$), and superoxide anion ($O_2^{-\cdot}$), which damage tissues by causing lipid peroxidation and DNA and protein injuries [1–3]. The ROS production, which was caused by $ROO^{\cdot}$ radicals, especially $HOO^{\cdot}/CH_3OO^{\cdot}$, is thought to play a role in the pathophysiology of aging and many age-related diseases, such as Alzheimer's disease (AD), cataracts, atherosclerosis, neoplastic diseases, diabetes, diabetic retinopathy, chronic inflammatory diseases of the gastrointestinal tract, aging of the skin, diseases of the cartilage, and chronic gastrointestinal tract diseases [4, 5]. The cellular sources of ROS and free radicals, and the clinical diseases linked to tissue damage and free radical generation. Furthermore, prospective therapeutic strategies for preventing damage caused by free radicals are considered. Numerous clinical diseases can be explained by harm caused by free radicals [4, 5].

The pharmacological computations can predict drug efficacies in humans, enhance their pharmacokinetic properties, find new targets, and minimize their side effects. In addition, the *in silico* methodology helps to reduce costs and expedite the entire design process. In recognition of the significance of the computational approach, employing density functional theory (DFT) to assess the medicinal possibilities of novel compounds exhibiting promising antiradical properties for AD treatment is encouraged.

Phlorotannins are natural compounds produced via the polymerization of 1,3,5-trihydroxybenzene (phloroglucinol). The structural classification depends on their monomeric units and linkages. For instance, fucols have only aryl–aryl connections, phlorethols and fuhalols have just ether, and fucophlorethols have both. It has been reported that they exist in almost orders of brown algae [6, 7]. They are essential to the ecosystem for wound healing, deterring fouling and herbivores, and providing defense against the harmful oxidative effects of UV light and warmth. These algal polyphenols have been the subject of current research as the food industry looks toward naturally sourced components to minimize the usage of synthetic food additives [6, 7]. Phlorotannins have been shown to have a high capacity for scavenging free radicals, suggesting that they are used as natural antioxidants in food preservation. Diphlorethol is a phlorotannin detected in the brown alga *Cystophora retroflexa* [8]. It falls into the class of phlorotannins with two phloroglucinol units connecting through an ether bond (Figure 1).

To get a better understanding of the role of phlorotannin derivatives, specifically diphlorethol, in antiradical actions, a DFT study was applied. This study mainly highlights the behavior of hydroxyl groups of diphlorethol, as well as the structural-electronic effects, thermochemical parameters, mechanisms of action, and kinetic reactions with the harmful $ROO^{\cdot}$ radicals. Molecular docking was used to examine the interactions between the studied molecule and the antioxidative Keap1 (human Kelch-like ECH-associated protein 1) protein. Furthermore, its significant efficacy in several living organs has also been taken into account with the ADMET profile.

2 | Methodology

2.1 | DFT Computational Study

The geometrical optimizations and frequency calculations were calculated using the Gaussian 09 package [9]. The M052X functional and 6-311++G(d,p) basis set were appropriate for kinetic considerations in radical scavenging mechanisms [10]. Compared to the popular functionals, such as M06-2X, M05-2X generally provides comparable or superior performance for radical-related processes, especially in gas-phase and noncovalent interactions [11, 12]. Both the thermochemical parameters bond dissociation energy (BDE), proton affinity (PA), and ionization potential (IP) and the kinetics have also been determined using the M052X/6-311++G(d,p) theoretical level in the gaseous phase, nonpolar medium pentyl ethanoate, and polar medium water [10]. The solvation model density (SMD), which was widely used for evaluating the radical scavenging activity of antioxidants, was used to compute the kinetic calculations under the QM-ORSA (quantum mechanics-based test for overall free radical scavenging activity) [10]. The number of imaginary frequencies was used to distinguish between local minima and transition state (TS), in which local minima only have real frequencies, but TS is indicated to contain one imaginary frequency. To ensure that the TS correctly connects the reactant complex (RC) and product complex (PC), an intrinsic reaction coordinate (IRC) calculation has been performed on both sides of the TS. The IRC final structures underwent additional optimizations to produce the fully relaxed geometry. The reaction kinetics calculation software used is the Eyringpy2.0 program [13].

Using the conventional transition state theory (TST) and 1-M standard state at 298.15 K, the rate constant k was expressed as Equation (1).

$$k = \sigma k \frac{k_B T}{h} e^{\frac{-\Delta G^{\neq}}{RT}} \tag{1}$$

where σ, k, k_B, h, R, T, and $\Delta G^{\neq}$ are the reaction path degeneracy, tunneling corrections, Boltzmann constant, Planck constant, molar gas constant, temperature, and Gibbs free energy of activation, respectively.

For the FHT mechanism, the $\Delta G^{\neq}$ was denoted as the Gibbs energy difference between TSs and reactants. Marcus's theory was employed in the SET reactions to view and study reaction barriers. The $\Delta G^{\neq}$ for the SET route related to the nuclear reorganization energy λ via Equations (2) and (3).

$$\Delta G_{SET}^{\neq} = \frac{\lambda}{4}\left(1 + \frac{\Delta G_{SET}^{0}}{\lambda}\right)^2 \tag{2}$$

$$\lambda \simeq \Delta E_{SET} - \Delta G_{SET}^{0} \tag{3}$$

where ΔE_{SET} stands for the non-adiabatic energy difference between the reactant and vertical product, and ΔG_{SET}^{0} represents the Gibbs energy of the reaction.

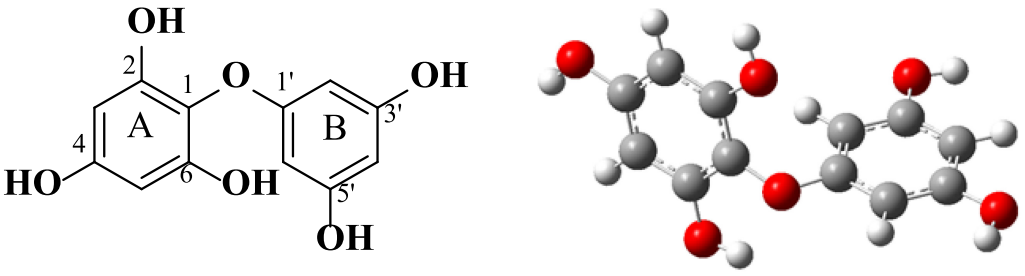

FIGURE 1 | Chemical structure of diphlorethol and its 3D-optimal form at the M052X/6-311++G(d,p) level of theory.

It noted that the reaction rate constant must be smaller than the diffusion limit. Therefore, it is desirable to reproduce the experimental values, the apparent rate constant k_{app} was considered (Equation 4), which is ruled by the Collins–Kimball theory [14].

$$k_{app} = \frac{k_D k}{k_D + k} \tag{4}$$

where k represents the thermal rate constant, and k_D stands for the steady-state Smoluchowski rate constant for an irreversible biomolecular diffusion-monitored reaction.

$$k_D = 4\pi R_{AB} D_{AB} N_A \tag{5}$$

where R_{AB} and N_A denote the reaction distance and Avogadro number, respectively. The mutual diffusion coefficient of reactant D_{AB} can be estimated from D_A and D_B, according to Truhlar [10, 15]. The D_A and D_B were predicted using the Stokes–Einstein approach (Equation 6).

$$D_{A\text{ or }B} = \frac{k_B T}{6\pi\eta a_{A\text{ or }B}} \tag{6}$$

where the viscosity η values of water and pentyl ethanoate are 8.9×10^{-4} and 8.62×10^{-4} Pa-s, respectively.

2.2 | Molecular Docking and ADMET

To understand the potential bindings (their binding positions and interactions) between diphlorethol and the antioxidative inhibitor Keap1, molecular docking simulations have been performed using the AutoDock Vina v1.2.5 program [16]. The crystal structure of Keap1 was obtained from the RCSB PDB with the PDB code 4L7B (https://www.rcsb.org) [17]. All the co-crystallized molecules (water, ions, and ligands) in the downloaded structure were removed using Chimera software. Subsequently, the polar hydrogen atoms and Gasteiger charges were assigned to Keap1 protein atoms to prepare the macromolecule using AutoDockTools v1.5.6 [18]. For ligand preparation, the 3D structures of diphlorethol and co-crystallized ligand (1*S*,2*R*)-2-{[(1*S*)-1-[(1,3-dioxo-1,3-dihydro-2*H*-isoindol-2-yl)methyl]-3,4-dihydroisoquinolin-2(1*H*)-yl]carbonyl}cyclohexanecarboxylic acid were optimized using Gaussian 09, and their files were saved in *.mol format using MarvinSketch software [9]. The ligands were then automatically assigned Gasteiger charges and torsion positions using AutoDockTools v1.5.6. Grid box parameters and grid point distances were determined based on the interaction positions of co-crystallized ligands with important amino acids in the active site using the GetBox plug-in in PyMOL (https://github.com/MengwuXiao/GetBox-PyMOL-Plugin). AutoDockTools were employed to analyze the binding affinity of protein-ligand docking, where lower energy indicates stronger binding. The interaction mode in the Keap1-diphlorethol complex was visualized using Discovery Studio Visualizer software. Additionally, the pharmacokinetic and ADMET parameters of the studied compound were evaluated using the pkCSM web server [19].

3 | Results and Discussion

3.1 | Geometry, Frontier Molecular Orbital Theory (FMO), Molecular Electrostatic Potential (MEP), Spin Density, and Fukui Analyses

Diphlorethol contains two phloroglucinol units connecting via an ether bridge. The π-electrons delocalize between the rings separately. At the M052X/6-311++G(d,p) theoretical level, the molecule deviates from planarity with the C1OC1′ bond angle of 117.80°. In all three studied mediums, the bond distances of OH groups have reached about 0.959 Å. As can be seen in the FMO illustration (Figure 2), the electrons were found to be delocalized in the whole molecule in the HOMO image of neutral form, but they highly focused on ring A in the LUMO image of neutral form. It suggests that the phenyl ring facilitates antioxidative reactions [9, 15]. The higher E_{HOMO} and the lower E_{LUMO} result in a better $E_{gap} = E_{HOMO} - E_{LUMO}$ [9, 15]. The E_{HOMO} is orderly run as pentyl ethanoate > gas > water (Table S1), whereas the E_{gap} runs as gas (0.302 eV) < pentyl ethanoate (0.306 eV) < water (0.311 eV). Therefore, the FHT mechanism will be preferential in weak/nonpolar media.

The charge density can be viewed by colors in the molecular electrostatic potential (MEP), in which red and yellow reflect electrophilic attack (excess electrons), blue is in contrast (the maximal positive charge), and green shows zero charges. Carbons and hydrogen atoms of diphlorethol are accompanied by green, and oxygen atoms mainly reveal yellow (Figure 2). Hence, OH groups may act as nucleophiles [20]. Generally, the spin density is evenly distributed in both phenyl rings (Figure 2). For instance, carbons C1, C3, and C5 contain positive charges, whereas carbons C2, C4, and C6 bear negative charges in the 4-OH radical case. It reinforces that two phenyl units would facilitate radical reactions. Importantly, the BDE values establish the same trend with the spin density [15, 20]. Herein, it is equivalent in the spin densities of 2-O˙ and 6-O˙ radicals. The spin densities of O˙ atoms in ring A are lower than those in ring B, suggesting the BDE values for 2-, 4-, and 6-OH are always less than those for 3- and 5-OH.

The Fukui parameters are also a useful key to get a better understanding of the reactivity of each atom. $\Delta f_t = f_t^+ - f_t^- < 0$ and > 0 represent the nucleophilicity and electrophilicity, respectively [15, 20]. From Table S2, all oxygen atoms showed nucleophilicity ($\Delta f_t < 0$), while some carbons, such as C4 and C5′, displayed electrophilicity. In another aspect, the $f_t^o < 0$ denotes the radical production. All OH groups exerted the negative f_t^o values or marginal zero. Expectedly, they are good sites for free radical scavenging.

3.2 | Thermodynamic Study

As can be seen from the literature, the thermodynamic parameters BDE, PA, and IP represent the antiradical mechanisms formal hydrogen transfer (FHT), sequential proton loss-electron transfer (SPLET), and single electron transfer-proton transfer (SET-PT), respectively [1–3, 15, 20]. These are calculated as Equations (7)–(9)

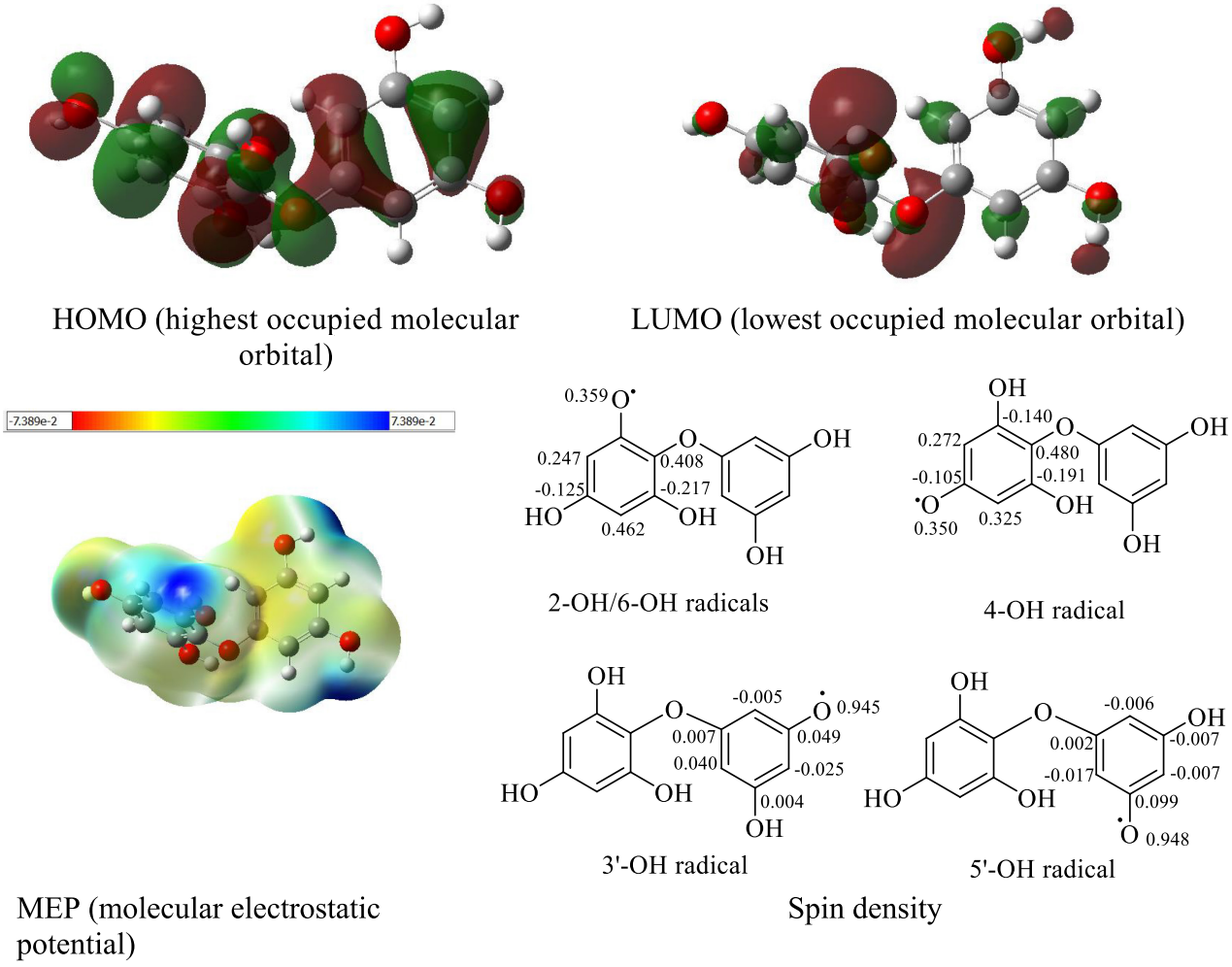

FIGURE 2 | The FMO, MEP, and spin density of diphlorethol in the gaseous phase at the M052X/6-311++G(d,p) level of theory.

$$\mathrm{BDE} = H\,(\mathrm{RO}^{\cdot}) + H(\mathrm{H}^{\cdot}) - H\,(\mathrm{ROH}) \tag{7}$$

$$\mathrm{PA} = H\,(\mathrm{RO}^{-}) + H\left(\mathrm{H}^{+}\right) - H\,(\mathrm{ROH}) \tag{8}$$

$$\mathrm{IP} = H\left(\mathrm{ROH}^{+\cdot}\right) + H(\mathrm{e}^{-}) - H\,(\mathrm{ROH}) \tag{9}$$

$$\mathrm{H(X)} = \mathrm{Eo} + \mathrm{ZPE} + \Delta\mathrm{H}_{\mathrm{trans}} + \Delta\mathrm{H}_{\mathrm{rot}} + \Delta\mathrm{H}_{\mathrm{vib}} + \mathrm{RT}$$

where H is the enthalpy of species (X), $\mathrm{E_O}$ and ZPE are electronic and zero-point energies, respectively. $\Delta\mathrm{H}_{\mathrm{trans}}$, $\Delta\mathrm{H}_{\mathrm{rot}}$, and $\Delta\mathrm{H}_{\mathrm{vib}}$ are translational, rotational, and vibrational distributions to enthalpy, respectively. The enthalpies of $H(\mathrm{e}^{-})$ and $H(\mathrm{H}^{+})$ are 0.75 and 1.48 kcal/mol in gas, −25.08 and −244.15 kcal/mol in water [2].

As shown in Table 1, the lowest gaseous BDE values of 87.1 to 87.9 kcal/mol were assigned to 4- and 6-OH, followed by 2-OH (91.6 kcal/mol), 3′-OH (108.2 kcal/mol), and 5′-OH (108.3 kcal/mol). This matches well with the spin density analysis. Also, in the gaseous phase, the IP and PA values are found much higher than the BDE values. Hence, the FHT route is the primary antiradical mechanism of the studied molecule in the gaseous phase [15, 20].

Considering solvent mediums, the BDE values of the studied OH groups in water range from 90 to 114.0 kcal/mol, and the pentyl ethanoate BDE values of 86.7–109.7 kcal/mol, and these BDE values are lower than the obtained IP values (120.5–133.4 kcal/mol). Especially, the PA values were found to be 32.6–25.4 and 59.9–63.9 kcal/mol in water and pentyl ethanoate, respectively. 6-OH has possessed the lowest PA values in both solvents (Table 1). It can be concluded that the SPLET is preferential for diphlorethol in the studied solvents [15, 20].

3.3 | Kinetic Study

3.3.1 | The Gaseous Reactions With $\mathrm{HOO}^{\cdot}/\mathrm{CH_3OO}^{\cdot}$ Radicals Following the FHT Mechanism

From the thermodynamic results, the antiradical action of diphlorethol in the gaseous medium was ruled by the FHT mechanism. Hence, its kinetics in the gas phase has been focused on the H-abstraction. Figures 3 and 4 illustrate the potential energy surfaces (PESs) and the optimal TSs, respectively. The reactant was first converted into RC and then formed TS. Before creating a product, TS has also been transformed into a PC. The barrier energies at the TSs ranged from 6.3 to 12.6 kcal/mol. In line with

TABLE 1 | The calculated enthalpies (kcal/mol) at the M052X/6-311++G(d,p) level of theory.

	Gas			Water			Pentyl ethanoate		
No	**BDE**	**PA**	**IP**	**BDE**	**PA**	**IP**	**BDE**	**PA**	**IP**
			178.8			120.5			133.4
2-OH	91.6	340.0		90.1	33.0		89.6	63.8	
4-OH	87.1	339.8		88.9	35.4		86.7	63.9	
6-OH	87.9	336.3		89.2	32.6		87.3	60.9	
3′-OH	108.2	332.2		114.1	34.9		109.6	60.5	
5′-OH	108.3	330.4		114.0	34.6		109.7	59.9	

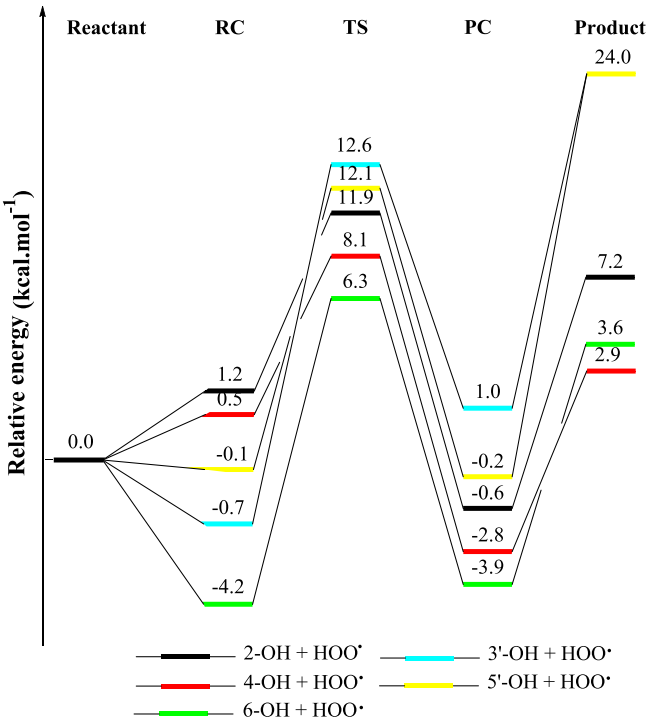

FIGURE 3 | Energy diagram for HOO˙ radical attack in the gaseous phase at the M052X/6-311++G(d,p) level of theory. PC: product complex, RC: reactant complex, TS: transition state.

the mentions above, 6-OH + HOO˙ gave the lowest relative energies at both RC, TS, and PC. Table 2 provides the obtained kinetic parameters. Herein, the lowest $\Delta G^{\neq}$ value of 15.3 kcal/mol, once again, was assigned to 6-OH + HOO˙, and this reaction also gave the highest k_{Eck} (rate constant) value of $4.93 \times 10^2 M^{-1} s^{-1}$. 4-OH + HOO˙ also marked with the low $\Delta G^{\neq}$ value and the high k_{Eck} value, whereas the remaining cases were not significant.

The lower activation energy for the 6-OH site compared to the 4-OH site can be attributed to the specific electronic environment and local stabilization effects. Particularly, the proton at the 6-OH position benefits from stabilization via intramolecular hydrogen bonding and favorable π-delocalization with the aromatic system, facilitating the interaction with the HOO˙ radical. Additionally, geometrical optimization revealed that the orientation of the 6-OH site allows for a more effective approach of the HOO˙ radical, thereby reducing the activation barrier.

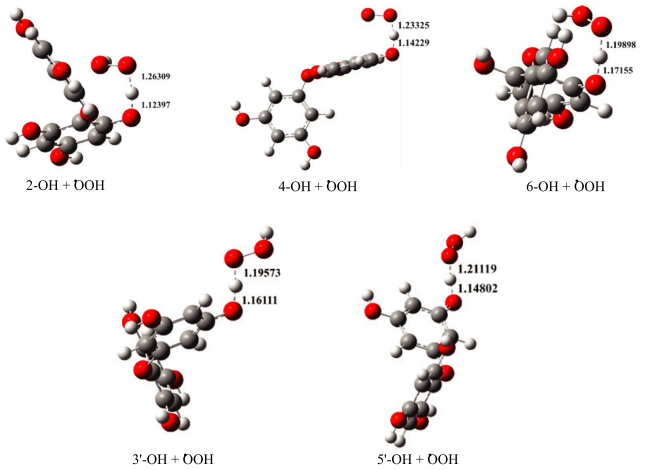

FIGURE 4 | The optimized transition state (TS) for HOO˙ radical attack in the gaseous phase at the M052X/6-311++G(d,p) level of theory following the FHT mechanism.

Regarding $CH_3OO˙$ radical scavenging (Figures 5 and 6 and Table 2), the barrier energies at the TSs were obtained with 6.3–12.8 kcal/mol. Besides the lowest TS energies, 4- and 6-OH also possessed the lowest $\Delta G^{\neq}$ values of 16.5–16.9 kcal/mol and the highest k_{Eck} values of 1.87×10^1–$5.96 \times 10^1 M^{-1} s^{-1}$. Meanwhile, the kinetic values of the remaining groups were insignificant. Collectively, the OH groups at carbons C-4 and C-6 are the most active sites for ROO˙ radical scavenging in the gaseous phase.

3.3.2 | The HOO˙/$CH_3OO˙$ Radical Scavenging in Physiological Environments

3.3.2.1 | **Acid–Base Equilibria.** Antiradical activity should be considered in physiological mediums that offer more accuracy and match well with experimental results. Hence, antiradical actions of diphlorethol were studied against ROO˙ in the water (pH = 7.4) and lipid (pentyl ethanoate that mimics polar and nonpolar mediums in the human body, respectively) [10, 14]. The understanding of protonation and deprotonation is important, and the pK_a and molar fraction f were calculated following the literature [21, 22]. From Table 3, the pK_a ranged from 8.54 to 9.20. The $f_{protonation}$ fluctuated from 0.932 to 0.989, whereas the $f_{deprotonation}$ reached from 0.0110 to 0.0680. These results clearly indicate that diphlorethol predominantly

TABLE 2 | Radical scavenging of diphlorethol in the gaseous phase at the M052X/6-311++G(d, p) level of theory.

	Diphlorethol + HOO˙			Diphlorethol + CH_3OO˙		
No	$\Delta G^{\neq}$	κ	k_{Eck}	$\Delta G^{\neq}$	κ	k_{Eck}
2-OH	20.8	23.3	8.43×10^{-2}	21.0	11.0	2.65×10^{-2}
4-OH	16.4	30.5	1.92×10^{2}	16.9	22.8	5.96×10^{1}
6-OH	15.3	13.5	4.93×10^{2}	16.5	3.8	1.87×10^{1}
3′-OH	20.4	0.0	1.38×10^{-12}	21.2	0.0	4.88×10^{-14}
5′-OH	20.0	0.0	1.20×10^{-12}	20.0	0.0	1.63×10^{-13}

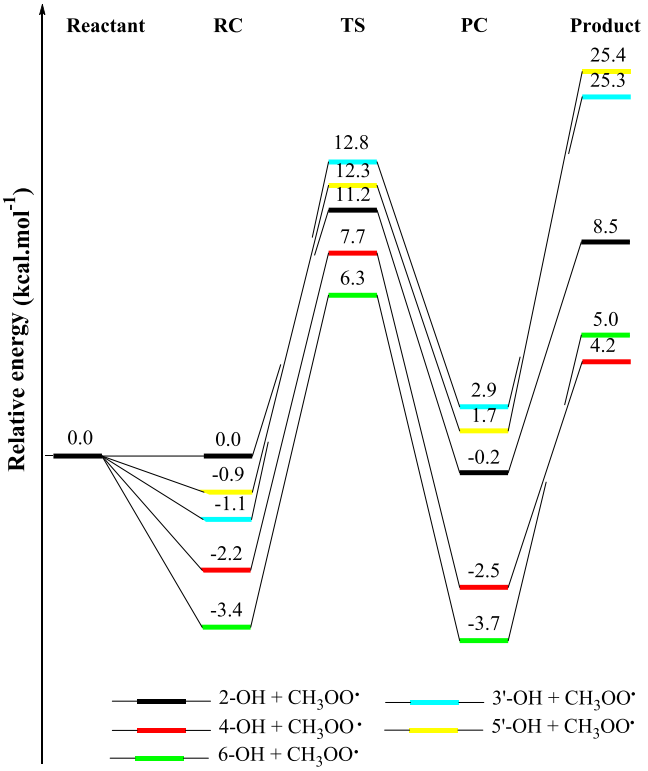

FIGURE 5 | Energy diagram for CH_3OO˙ radical attack in the gaseous phase at the M052X/6-311++G(d,p) level of theory.

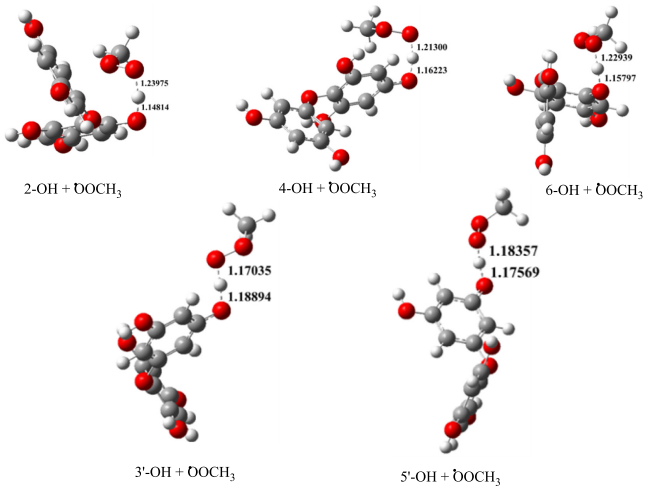

FIGURE 6 | The optimized TS for CH_3OO˙ radical attack in the gaseous phase at the M052X/6-311++G(d,p) level of theory following the FHT mechanism.

TABLE 3 | The calculated pK_a and f (pH = 7.4) at the M052X/6-311++G(d, p) level of theory.

No	pK_a	$f_{protonation}$ (ROH)	$f_{deprotonation}$ (RO^-)
2-OH	8.65	9.47×10^{-1}	5.30×10^{-2}
4-OH	9.35	9.89×10^{-1}	1.10×10^{-2}
6-OH	8.54	9.32×10^{-1}	6.80×10^{-2}
3′-OH	9.20	9.84×10^{-1}	1.60×10^{-2}
5′-OH	9.00	9.75×10^{-1}	2.50×10^{-2}

exists in its neutral form in water at pH 7.4, with a minor contribution from its deprotonated form. Although the extent of deprotonation is relatively low, both protonation states were considered in the subsequent kinetic studies to ensure accuracy. In contrast, for simulations in pentyl ethanoate representing the lipid environment of biological systems, the neutral form was exclusively used, given the non-ionizing nature of the solvent. This approach ensures that the modeling of diphlorethol's antiradical behavior in both polar and non-polar biological environments is comprehensive and aligned with physiological relevance.

3.3.2.2 | **Kinetic Study.** The kinetic reaction between diphlorethol and ROO˙ radicals in the water was elucidated using the FHT route for neutral states and the SET route for anion states [10, 12]. This is consistent with the thermodynamic results that the neutral states only happened following the FHT pathway at similar positions in the gaseous phase.

Thus, the overall rate constant ($k_{overall}$) in the lipid medium was determined as Equation (10)

$$k_{overall} = \sum k_{app}^{FHT}(ROH) \tag{10}$$

And the $k_{overall}$ in the aqueous medium (Equation 11)

$$\begin{aligned} k_{overall} &= fk_{app}^{SET}(RO^-) + fk_{app}^{FHT}(ROH) \\ &= k_{app}^{SET}(RO^-) + k_{app}^{FHT}(ROH) \end{aligned} \tag{11}$$

The branching ratio (Γ), which was a contribution of each reaction mechanism in the overall rate constant, was computed following Equation (12).

$$\Gamma = (k \times 100) / k_{overall} \quad (12)$$

Regarding diphlorethol + HOO˙ (Table 4 and Figures S1 and S2), the $k_{overall}$ in the aqueous medium is $1.6 \times 10^8\,M^{-1}s^{-1}$, which is much larger than that in the lipid medium ($k_{overall} = 2.7 \times 10^1\,M^{-1}s^{-1}$). Significantly, the SET mechanism is predominant in the aqueous medium with the $\Gamma = 100\%$, whereas the FHT is preferential in the lipid (6-OH + HOO˙, $\Gamma = 73.75\%$; 4-OH + HOO˙, $\Gamma = 73.75\%$; and 2-OH + HOO˙, $\Gamma = 0.07\%$).

In the same manner, the studied molecule quickly reacted with CH_3OO˙ in the water with the $k_{overall}$ value of $1.20 \times 10^8\,M^{-1}s^{-1}$, which is monitored by the SET mechanism ($\Gamma = 100\%$) (Table 5 and Figures S3 and S4). The FHT route is essential for diphlorethol + CH_3OO˙ in the medium pentyl ethanoate with the $k_{overall}$ value of $3.0 \times 10^0\,M^{-1}s^{-1}$. It is also observed that the OH groups at carbons C-4 and C-6 mainly contributed to these results, with the Γ values of 36.61% and 63.24%, respectively.

At the same condition of pH = 7.4 and M052X/6-311++G(d,p) theoretical level, the standard compound trolox reacted with HOO˙ radicals in the water with the $k_{overall}$ value of $2.47 \times 10^3\,M^{-1}s^{-1}$ [23]. Reactions of trolox and α-tocopherol with CH_3OO˙ in the pentyl ethanoate at M062X/6-311++G(d,p) level resulted in the $k_{overall}$ values of 5.5×10^8 and $2.63 \times 10^7\,M^{-1}s^{-1}$, respectively [23]. At the same M062X/6-311++G(d,p) level, the other well-known antioxidant butylated hydroxytoluene reacted with HOO˙ radicals in the water, and lipid exerted the $k_{overall}$ values of 2.51×10^5 and $1.70 \times 10^4\,M^{-1}s^{-1}$, respectively [24]. As a consequence, the phytochemical class of phlorotannins, such as diphlorethol, is also appropriate for antioxidant activities.

3.4 | Molecular Docking and ADMET

As we know, the Keap1-Nrf2 signaling pathway is crucial for both self-defense and defense against endogenous and exogenous oxidative stresses [25]. In normal conditions, Keap1 can bind to Nrf2 and facilitate its degradation, thereby blocking the response of the antioxidant system to stress. On the other hand, antioxidant molecules bind to Keap1 Kelch domain, and obstruct the Keap1-Nrf2 interaction, thereby blocking the Keap1-Nrf2 pathway and successfully triggering the antioxidant pathway [26]. The co-crystallized ligand (1*S*,2*R*)-2-{[(1*S*)-1-[(1,3-dioxo-1,3-dihydro-2*H*-isoindol-2-yl)methyl]-3,4-dihydroisoquinolin-2(1*H*)-yl]carbonyl}cyclohexanecarboxylic acid interacts to the Keap1 Kelch domain with key amino acid residues, including Arg415, Ser602, Asn414, Tyr334, Ala556, and Tyr572 [17]. With the aid of

TABLE 4 | The calculated $\Delta G^{\neq}$ (Gibbs free energy of activation, kcal mol^{-1}), k_{app} (apparent rate constant, $M^{-1}s^{-1}$), f (molar fraction), k_f (rate constant included pH effect, $M^{-1}s^{-1}$), and Γ (branching ratio, %) of diphlorethol + HOO˙ reaction at the M052X/6-311++G(d, p) level of theory.

		Water					Pentyl ethanoate		
Mechanism	**No**	$\Delta G^{\neq}$	k_{app}	**f**	k_f	Γ	$\Delta G^{\neq}$	k_{app}	Γ
SET		2.2	2.4×10^9	6.76×10^{-2}	1.6×10^8	100.00			
FHT	2-OH	20.9	1.8×10^1	5.30×10^{-2}	9.5×10^{-1}	0.00	22.8	1.8×10^{-2}	0.07
	4-OH	20.3	1.3×10^1	1.10×10^{-2}	1.4×10^{-1}	0.00	19.4	7.1×10^0	26.18
	6-OH	20.4	2.2×10^1	6.80×10^{-2}	1.5×10^0	0.00	18.9	2.0×10^1	73.75
	3′-OH	21.0	1.8×10^{-15}	1.60×10^{-2}	2.8×10^{-17}	0.00	23.0	4.4×10^{-13}	0.00
	5′-OH	22.2	2.8×10^{-15}	2.50×10^{-2}	6.9×10^{-17}	0.00	23.2	3.4×10^{-13}	0.00
$k_{overall}$			1.6×10^8				$k_{overall}$	2.7×10^1	

TABLE 5 | The calculated $\Delta G^{\neq}$ (in kcal mol^{-1}), k_{app} ($M^{-1}s^{-1}$), and Γ (%) of diphlorethol + CH_3OO˙ reaction at the M052X/6-311++G(d, p) level of theory.

		Water					Pentyl ethanoate		
Mechanism	**No**	$\Delta G^{\neq}$	k_{app}	**f**	k_f	Γ	$\Delta G^{\neq}$	k_{app}	Γ
SET		3.9	1.7×10^9	6.76×10^{-2}	1.2×10^8	100			
FHT	2-OH	22.3	1.2×10^0	5.32×10^{-2}	6.5×10^{-2}	0.00	23.7	4.3×10^{-3}	0.15
	4-OH	21.2	1.0×10^0	1.11×10^{-2}	1.1×10^{-1}	0.00	20.5	1.1×10^0	36.61
	6-OH	21.8	3.5×10^0	6.76×10^{-2}	2.3×10^{-1}	0.00	19.5	1.9×10^0	63.24
	3′-OH	21.7	3.2×10^{-16}	1.56×10^{-2}	7.7×10^{-18}	0.00	24.7	1.9×10^{-15}	0.00
	5′-OH	21.9	9.7×10^{-17}	2.45×10^{-2}	1.5×10^{-18}	0.00	24.2	3.0×10^{-15}	0.00
$k_{overall}$			1.20×10^8				$k_{overall}$	3.0×10^0	

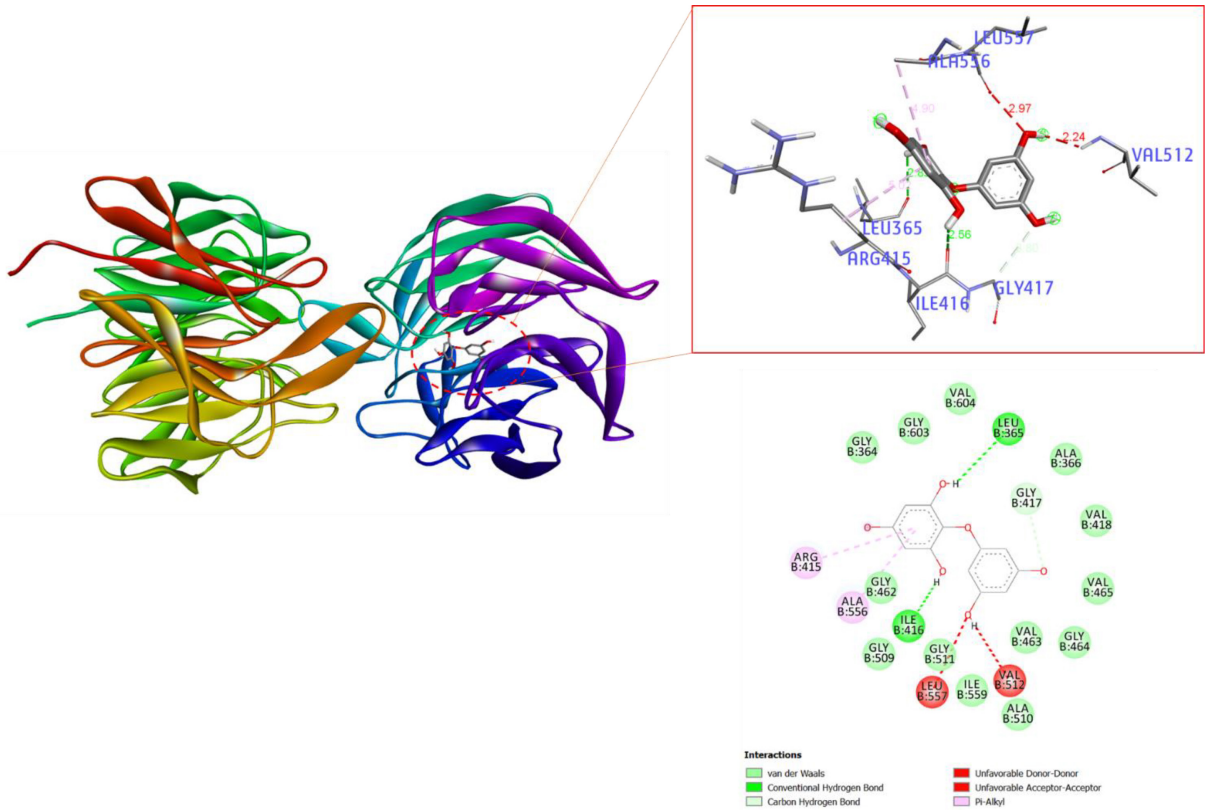

FIGURE 7 | Molecular docking results of interactions between diphlorethol and Keap1 (PDB ID: 4L7B).

molecular docking, one can rapidly determine the ideal score function value for every protein interacting with a ligand. Any docking calculation seeks to identify the optimal pose, or the one with the lowest energy [27]. The docking result is reliable with a root-mean-square deviation (RMSD) of less than 2.0 Å [28–30]. In this work, the RMSD value of the co-crystallized ligand, which was 0.717 Å, was used to compare its docked pose, which had the lowest binding free energy, with its native structure (Figure S5). This outcome showed that the process was repeatable, and the parameters were suitable for additional docking simulations [28–30]. Therefore, diphlorethol was docked into the active site of the Keap1 Kelch domain, and the analysis was conducted using AutoDock Vina v1.2.5 to assess its potential antioxidant activity through the Keap1-Nrf2 pathway. The binding modes of diphlorethol to human Keap1 are illustrated in Figure 7. Diphlorethol has shown an estimated binding affinity of −7.569 kcal/mol, thereby forming hydrogen bonds with Leu365 and Ile416. Additionally, this compound engages in π-alkyl interactions between the benzene ring of the molecule and the carbon atoms of Ala556 and Arg415. It is noteworthy that the residue Arg415 plays a crucial role in inhibiting the Keap1 domain [17].

Besides pharmacological evaluation, it is necessary to consider the metabolic progress of a molecule in living bodies. The pkCSM web platform has been utilized to consider substances' adsorption, including skin permeability (logKp), intestinal adsorption, water solubility, transdermal absorption using Caco-2 cell models (logPapp), and skin solubility (logPapp). The parameters for the penetration of the central nervous system (logPS), blood–brain barrier permeability (logBB), and VDss were determined to ascertain the in silico distribution of the substances under investigation. In addition, several toxicity indicators for the substances under test were computed, including the maximum tolerated dose, skin sensitization, acute and chronic oral rat toxicity, *Tetrahymena pyriformis* toxicity, and minnow toxicity. Diphlorethol has a good water solubility with a logP value of −3.265 (Table 6). It is assumed that a compound with low Caco-2 permeability is associated with a logPapp of less than 0.9. Herein, the logPapp of 0.302 was assigned to diphlorethol. This molecule also exhibited a high intestinal absorption capability (> 30%) with a predicted value of the absorbed 74.067%. Its skin permeability is good, with a logKp value lower than −2.5 (logKp = −2.735). The logVDss parameter of 0.162 reflected that diphlorethol might be characterized by a relatively even distribution in tissues. According to the model used in the pkCSM software, VDss is considered high with a logVDss of more than 0.45 and low with a logVDss of less than −0.15. A higher VDss indicated greater drug distribution into tissues compared to serum.

Diphlorethol testing also revealed the values of logBB and logPS parameters indicating poor blood–brain barrier penetration (logBB < −1), specifically with a value of −1.266, and poor penetration into the central nervous system (logPS > −2) with a logPS value of −3.357. In terms of metabolism, diphlorethol is not a substrate for CYP2D6 and CYP3A4. Furthermore, this molecule did not inhibit any of the predicted cytochrome P450 isoforms (CYP1A2, CYP2C19, CYP2C9, CYP2D6, and CYP3A4). The total drug clearance, measured by the

TABLE 6 | The predicted ADME parameters.

Property	Model name	Predicted value	Unit
Absorption	Water solubility	−3.265	Numeric (log mol/L)
Absorption	Caco2 permeability	0.302	Numeric (logPapp in 10^{-6} cm/s)
Absorption	Intestinal absorption (human)	74.067	Numeric (absorbed %)
Absorption	Skin permeability	−2.735	Numeric (logKp)
Absorption	P-glycoprotein substrate	Yes	Categorical (yes/no)
Absorption	P-glycoprotein I inhibitor	No	Categorical (yes/no)
Absorption	P-glycoprotein II inhibitor	No	Categorical (yes/no)
Distribution	VDss (human)	0.162	Numeric (logL/kg)
Distribution	Fraction unbound (human)	0.143	Numeric (Fu)
Distribution	BBB permeability	−1.266	Numeric (logBB)
Distribution	CNS permeability	−3.357	Numeric (logPS)
Metabolism	CYP2D6 substrate	No	Categorical (yes/no)
Metabolism	CYP3A4 substrate	No	Categorical (yes/no)
Metabolism	CYP1A2 inhibitor	No	Categorical (yes/no)
Metabolism	CYP2C19 inhibitor	No	Categorical (yes/no)
Metabolism	CYP2C9 inhibitor	No	Categorical (yes/no)
Metabolism	CYP2D6 inhibitor	No	Categorical (yes/no)
Metabolism	CYP3A4 inhibitor	No	Categorical (yes/no)
Excretion	Total clearance	0.664	Numeric (log mL/min/kg)
Excretion	Renal OCT2 substrate	No	Categorical (yes/no)
Toxicity	AMES toxicity	Yes	Categorical (yes/no)
Toxicity	Max. tolerated dose (human)	0.901	Numeric (log mg/kg/day)
Toxicity	hERG I inhibitor	No	Categorical (yes/no)
Toxicity	hERG II inhibitor	No	Categorical (yes/no)
Toxicity	Oral rat acute toxicity (LD_{50})	1.89	Numeric (mol/kg)
Toxicity	Oral rat chronic toxicity (LOAEL)	3.381	Numeric (log mg/kg bw/day)
Toxicity	Hepatotoxicity	No	Categorical (yes/no)
Toxicity	Skin sensitization	No	Categorical (yes/no)
Toxicity	*Tetrahymena pyriformis* toxicity	0.323	Numeric (log ug/L)
Toxicity	Minnow toxicity	0.713	Numeric (log mM)

predicted CLtot value for diphlorethol, is 0.664 log mL/min/kg. Regarding toxicity, the pkCSM platform indicated that diphlorethol did not induce toxicity in the liver and skin and also did not inhibit the hERGs I and II. However, in the AMES prediction, there is an indication of mutagenic potential for the compound. The Oral Rat Acute Toxicity LD_{50} value for the tested substances is 1.89 mol/kg, and the LOAEL parameter is 3.381 log mg/kg bw/day (Table 6). By combining information from the pkCSM platform, these results provide insights into the pharmacokinetic properties of diphlorethol, and shape the direction of development in the field of pharmaceutical research.

4 | Conclusion

Computational calculations were applied to evaluate the antiradical action of diphlorethol against $HOO^{\cdot}$ and $CH_3OO^{\cdot}$ radicals. The results revealed that the FHT pathway is essential for its antiradical activity in nonpolar/weak media. In the meantime, the SET mechanism is preferential in polar media. Radical scavenging is related to the great role of OH groups at two carbons, C-4 and C-6. Moreover, the docking results revealed a parallel pathway for diphlorethol's antioxidant properties, suggesting its potential to inhibit Keap1 enzyme activity in response to both endogenous and exogenous oxidative stresses.

Author Contributions

Chu Anh Van and **Tran Quang Hai:** analyzed the data and prepared the figures. **Nguyen Thi Hanh** and **Nguyen Ngoc Linh:** data curation. **Ninh The Son:** supervised and wrote the manuscript. All authors have read and approved this submission.

Conflicts of Interest

The authors declare no conflicts of interest.

Data Availability Statement

The data that support the findings of this study are available in the figures, tables, and the Supporting Information section of this article.

References

1. P. T. Thuy, T. T. Hieu, D. X. Duc, et al., "Antioxidative Limonoids From *Swietenia macrophylla* Fruits: Experimental, DFT (Density Functional Theory) Approach, and Docking Study," *Journal of Molecular Structure* 1283 (2023): 135264, https://doi.org/10.1016/j.molstruc.2023.135264.

2. N. T. Son, P. T. Thuy, and N. V. Trang, "Suaveolensone B: A Detailed Analysis of Structural-Electronic Properties and Mechanisms," *Journal of Molecular Structure* 1224 (2021): 129025, https://doi.org/10.1016/j.molstruc.2020.129025.

3. C. Kaur and D. Mandal, "Insights Into the HO· and HOO· Radical Scavenging Activity of Aryl Carbamate Derivative: A Computational Mechanistic and Kinetic Investigation," *Theoretical Chemistry Accounts* 143 (2024): 28, https://doi.org/10.1007/s00214-024-03102-3.

4. S. Yang and G. Lian, "ROS and Diseases: Role in Metabolism and Energy Supply," *Molecular and Cellular Biochemistry* 467 (2020): 1–12, https://doi.org/10.1007/s11010-019-03667-9.

5. Z. Liu, Z. Ren, J. Zhang, et al., "Role of ROS and Nutritional Antioxidants in Human Diseases," *Frontiers in Physiology* 9 (2018): 477, https://doi.org/10.3389/fphys.2018.00477.

6. D. A. Kirke, T. J. Smyth, D. K. Rai, O. Kenny, and D. B. Stengel, "The Chemical and Antioxidant Stability of Isolated Low Molecular Weight Phlorotannins," *Food Chemistry* 221 (2017): 1104–1112, https://doi.org/10.1016/j.foodchem.2016.11.050.

7. H. M. Mwangi, J. Van Der Westhuizen, J. Marnewick, W. T. Mabusela, M. M. Kabanda, and E. E. Ebenso, "Isolation, Identification and Radical Scavenging Activity of Phlorotannin Derivatives From Brown Algae, *Ecklonia maxima*: An Experimental and Theoretical Study," *Free Radicals and Antioxidants* 3 (2013): S1–S10, https://doi.org/10.1016/j.fra.2013.10.006.

8. S. Birgit and G. Karl-werner, "Phlorethols and Fucophlorethols Form the Brown Alga *Cystophora retroflexa*," *Phytochemistry* 50 (1999): 869–881, https://doi.org/10.1016/S0031-9422(98)00643-8.

9. P. T. Thuy, D. X. Duc, and N. T. Son, "A Comparative DFT Study on Antioxidative Activity of 3- and 4-Phenylcoumarins: An Aspect of Structure, Electronics, Mechanism, Kinetics, and Metal Chelate Relations," *Structural Chemistry* 35 (2024): 265–275, https://doi.org/10.1007/s11224-023-02183-3.

10. V. V. Quan, N. M. Thong, T. L. Huyen, et al., "A Thermodynamic and Kinetic Study of the Antioxidant Activity of Natural Hydroanthraquinones," *RCS Advances* 10 (2020): 20089, https://doi.org/10.1039/D0RA04013D.

11. E. G. Hohenstein, S. T. Chill, and C. D. Sherrill, "Assessment of the Performance of the M05-2X and M06-2X Exchange-Correlation Functionals for Noncovalent Interactions in Biomolecules," *Journal of Chemical Theory and Computation* 4 (2008): 1996–2000, https://doi.org/10.1021/ct800308k.

12. A. Bayat and A. Fattahi, "A Quantum Chemical Study on the OH Radical Quenching by Natural Antioxidant Fisetin," *Journal of Physical Organic Chemistry* 30 (2017): e3692, https://doi.org/10.1002/poc.3692.

13. E. Dzib, J. L. Cabellos, F. Ortíz-Chi, S. Pan, A. Galano, and G. Merino, "Eyringpy: A Program for Computing Rate Constants in the Gas Phase and in Solution," *International Journal of Quantum Chemistry* 119 (2019): e25686, https://doi.org/10.1002/qua.25686.

14. M. V. Bay, P. C. Nam, N. T. Hoa, A. Mechler, and Q. V. Vo, "Antiradical Activity of Lignans From *Cleistanthus sumatranus*: Theoretical Insights Into the Mechanism, Kinetics, and Solvent Effects," *ACS Omega* 8 (2023): 38668–38675, https://doi.org/10.1021/acsomega.3c05964.

15. P. T. Thuy, N. V. Trang, D. X. Duc, N. Van Trang, and N. T. Son, "The Antioxidative Potential of Benzofuran-Stilbene Hybrid Derivatives: A Comparison Between Natural and Synthetic Compounds," *Structural Chemistry* 32 (2021): 2271–2281, https://doi.org/10.1007/s11224-021-01802-1.

16. J. Eberhardt, D. Santos-Martins, A. F. Tillack, and S. Forli, "AutoDock Vina 1.2. 0: New Docking Methods, Expanded Force Field, and Python Bindings," *Journal of Chemical Information and Modeling* 61 (2021): 3891–3898, https://doi.org/10.1021/acs.jcim.1c00203.

17. E. Jnoff, C. Albrecht, J. J. Barker, et al., "Binding Mode and Structure-Activity Relationships Around Direct Inhibitors of the Nrf2–Keap1 Complex," *ChemMedChem* 9 (2014): 699–705, https://doi.org/10.1002/cmdc.201300525.

18. G. M. Morris, R. Huey, W. Lindstrom, et al., "AutoDock4 and AutoDockTools4: Automated Docking With Selective Receptor Flexibility," *Journal of Computational Chemistry* 30 (2009): 2785–2791, https://doi.org/10.1002/jcc.21256.

19. D. E. Pires, T. L. Blundell, and D. B. Ascher, "pkCSM: Predicting Small-Molecule Pharmacokinetic and Toxicity Properties Using Graph-Based Signatures," *Journal of Medicinal Chemistry* 58 (2015): 4066–4072, https://doi.org/10.1021/acs.jmedchem.5b00104.

20. P. T. Thuy, P. M. Quan, D. X. Duc, and N. T. Son, "The Antioxidative Potential of Procyanidin B1: DFT (Density Functional Theory) and Docking Approaches," *Journal of Molecular Modeling* 28 (2022): 356, https://doi.org/10.1007/s00894-022-05354-x.

21. A. Galano and J. R. Alvarez-Idaboy, "A Computational Methodology for Accurate Predictions of Rate Constants in Solution: Application to the Assessment of Primary Antioxidant Activity," *Journal of Computational Chemistry* 34 (2013): 2430–2445, https://doi.org/10.1002/jcc.23409.

22. A. Galano, A. D. Pérez-González, R. Castañeda-Arriaga, et al., "Empirically Fitted Parameters for Calculating pKa Values With Small Deviations From Experiments Using a Simple Computational Strategy," *Journal of Chemical Information and Modeling* 56 (2016): 1714–1724, https://doi.org/10.1021/acs.jcim.6b00310.

23. A. Amić and D. Mastil'ak Cagardova, "A DFT Study of the Antioxidant Potency of α-Tocopherol and Its Derivatives: PMHC, Trolox, and α-CEHC," *Journal of Molecular Liquids* 403 (2024): 124796, https://doi.org/10.1016/j.molliq.2024.124796.

24. H. Boulebd, "Radical Scavenging Behavior of Butylated Hydroxytolunene Against Oxygenated Free Radicals in Physiological Enviroments: Insights From DFT Calculations," *International Journal of Chemical Kinetics* 54 (2022): 50–57, https://doi.org/10.1002/kin.21540.

25. M. Yang, Z. H. Jiang, C. G. Li, et al., "Apigenin Prevents Metabolic Syndrome in High-Fructose Diet-Fed Mice by Keap1-Nrf2 Pathway," *Biomedicine & Pharmacotherapy* 105 (2018): 1283–1290, https://doi.org/10.1016/j.biopha.2018.06.108.

26. S. C. Lo, X. Li, M. T. Henzl, L. J. Beamer, and M. Hannink, "Structure of the Keap1: Nrf2 Interface Provides Mechanistic Insight Into Nrf2 Signaling," *EMBO Journal* 25 (2006): 3605–3617, https://doi.org/10.1038/sj.emboj.7601243.

27. L. M. Berezhkovskiy, "Prediction of Drug Terminal Half-Life and Terminal Volume of Distribution After Intravenous Dosing Based on Drug Clearance, Steady-State Volume of Distribution, and Physiological Parameters of the Body," *Journal of Pharmaceutical Sciences* 102 (2013): 761–771, https://doi.org/10.1002/jps.23396.

28. N. T. Tra, N. X. Ha, N. V. Tuyen, et al., "Essential Oils of Alpinia Vietnamica Rhizomes and Leaves: Chemical Composition, Cytotoxicity, α-Glucosidase Inhibition, and Molecular Docking Approach," *Natural Product Communications* 18 (2023): 1–12, https://doi.org/10.1177/1934578X231206280.

29. B. Guan, C. Zhang, and Y. Zhao, "An Efficient ABC_DE_Based Hybrid Algorithm for Protein-Ligand Docking," *International Journal of Molecular Sciences* 19 (2018): 1181, https://doi.org/10.3390/ijms19041181.

30. C. Guibert and T. L. James, "Docking to RNA via Root-Mean-Square-Deviation-Driven Energy Minimization With Flexible Ligands and Flexible Targets," *Journal of Chemical Information and Modeling* 48 (2008): 1257–1268, https://doi.org/10.1021/ci8000327.

Supporting Information

Additional supporting information can be found online in the Supporting Information section.